The American Journal of Pathology, Vol. 175, No. 1, July 2009

DOI: 10.2353/ajpath.2009.080870

Cardiovascular, Pulmonary and Renal Pathology

Complex Integration of Matrix, Oxidative Stress, and Apoptosis in Genetic Emphysema

Megan Podowski,* Carla L. Calvi,* Christopher Cheadle,† Rubin M. Tuder,‡ Shyam Biswals,§ and Enid R. Neptune*

From the Divisions of Pulmonary and Critical Care Medicine, Rheumatology,† and Cardiopulmonary Pathology,‡ Johns Hopkins University School of Medicine, Baltimore; and the Department of Environmental Health Sciences,§ Johns Hopkins School of Public Health, Baltimore, Maryland*

Alveolar enlargement, which is characteristic of bronchopulmonary dysplasia, congenital matrix disorders, and cigarette smoke-induced emphysema, is thought to result from enhanced inflammation and ensuing excessive matrix proteolysis. Although there is recent evidence that cell death and oxidative stress punctuate these diseases, the mechanistic link between abnormal lung extracellular matrix and alveolar enlargement is lacking. We hypothesized that the tight-skin (TSK) mouse, which harbors a spontaneous internal duplication in the microfibrillar glycoprotein fibrillin-1, might show whether matrix alterations are sufficient to promote oxidative stress and cell death, injury cascades central to the development of clinical emphysema. We observed no evidence of increased metalloprotease activation by histochemical and zymographic methods. We did find initial oxidative stress followed by increased apoptosis in the postnatal TSK lung. Both blunted antioxidant production and reduced extracellular superoxide dismutase activity were evident in the neonatal lung. High-dose antioxidant treatment with *N*-acetylcysteine improved airspace caliber and attenuated oxidative stress and apoptosis in neonatal and adult TSK mice. These data establish that an abnormal extracellular matrix without overt elastolysis is sufficient to confer susceptibility to postnatal normoxia, reminiscent of bronchopulmonary dysplasia. The resultant oxidative stress and apoptosis culminate in profound airspace enlargement. The TSK lung exemplifies the critical interplay between extracellular matrix, oxidative stress, and cell-death cascades that may contribute to genetic and acquired airspace enlargement. ***(Am J Pathol 2009, 175:84–96; DOI: 10.2353/ajpath.2009.080870)***

Alveolarization, or the formation of alveolar sacs, provides the extensive surface for gas exchange that is required for the proper function of all vertebrate lungs. A precise temporospatial series of molecular cues and responses induce the proliferative, migratory, and differentiation events that punctuate alveolar formation. This process not only serves a developmental function, but must also be reiterated in reparative contexts (nicely reviewed in[1,2]). The extracellular matrix assumes both structural and inductive roles in airspace formation and maintenance. Several murine models with dysregulated matrix production or turnover display airspace phenotypes that approximate the histology of acquired emphysema or bronchopulmonary dysplasia.[3–8] However, whether an abnormal matrix is sufficient to trigger canonical injury cascades in the airspace compartment is unknown. The current study examines the specific connection between an abnormal matrix element and airspace homeostasis.

The four cardinal histological findings in human cigarette smoke-induced emphysema are 1) airspace enlargement, 2) aberrant matrix turnover, 3) oxidative stress, and 4) chronic inflammation. Because these manifestations are interrelated and because cigarette smoke, the proximal trigger, can directly or indirectly promote all of these signatures, a clear demonstration of the early critical events that initiate the destructive cascade is lacking. Spontaneous or genetically targeted mutant mice with emphysema provide a unique set of tools to investigate the validity of a "critical-trigger" pathogenetic

Supported in part by the National Institutes of Health (grants KO8-HL067980 and RO1-HL085312 to E.R.N., grant RO1-HL066554 to R.T., grant RO1-HL081205 to S.B., and grant SCCOR P50HL074945 to E.R.N., R.T. and S.B.); Alpha-One Foundation Grant to R.T., and the March of Dimes Basil O'Connor Award to E.R.N.

M.P. and C.L.C. contributed equally to this work.

Accepted for publication April 3, 2009.

Supplemental material for this article can be found on *http://ajp.amjpathol.org*.

Current affiliation for R.M.T.: Program in Translational Lung Research, Division of Pulmonary Sciences and Critical Care Medicine, Department of Medicine, University of Colorado.

Address reprint requests to Enid R. Neptune, M.D., Johns Hopkins University School of Medicine, 1830 East Monument St., Room 547, Baltimore, MD 21205. E-mail: eneptune@jhmi.edu.

cascade. The TSK mouse, a well-studied, spontaneous mutant model of cutaneous fibrosis and genetic emphysema, provides important insight into the pathophysiology of emphysematous airspace simplification, since its single spontaneous genetic insult is an alteration in a microfibrillar protein, but its adult phenotype encompasses all of the signature features of human emphysema.[9] These mice carry a spontaneous internal duplication in fibrillin-1, a ubiquitous extracellular matrix glycoprotein, which results in a large abnormal fibrillin that is incorporated into the microfibrillar lattice of the extracellular matrix.[10] Thus, in the TSK lung, an alteration in the structure but not expression of a matrix protein is sufficient to induce the full phenotype of airspace enlargement and chronic inflammation.

The origin of the airspace lesion in the TSK lung, which is punctuated by neonatal septation defects that progress into adulthood, is controversial. The proposed mechanisms for the TSK airspace phenotype include 1) excessive protease activity, 2) mechanical forces superimposed on a fragile tissue, 3) inflammation, and 4) abnormal matrix deposition or remodeling, all of which have been postulated to contribute to cigarette smoke-induced emphysema. In an elegant study, Martorana et al performed a detailed time-course of the airspace lesion in these mice and described an initial alveolar septation defect resulting in airspace enlargement followed by overt airspace destruction in the adult TSK lung.[11] Despite reports of increased elastase expression in the serum and lungs of TSK mice,[12,13] no evidence of increased local protease activation has been observed.[14] Several groups have shown increases in collagen deposition in the adult TSK lung but variably accompanied by reduced elastin content.[15] Since exuberant protease activation is thought critical for matrix remodeling in cigarette smoke-induced emphysema, how the airspace findings in the TSK lung might proceed from the primary abnormality in matrix composition is unclear. Suki recently proposed a model of abnormal collagen remodeling in the TSK lung which results not in fibrosis but in increased hysteresivity and "dynamic nonlinearity" culminating in septal breakdown secondary to overstretched airspaces.[16] Initial enthusiasm for an inflammatory basis for the lesion, involving inflammatory cell mediated local proteolysis,[17] was tempered by the findings that crossing the TSK allele into a lymphocyte depleted background or into a neutrophil-elastase deficient strain[18] did not rescue the lung phenotype. Furthermore, the documentation of parenchymal lung inflammation has been inconsistent. Although Szapiel found a mild macrophage-neutrophil alveolitis,[17] others have not detected inflammation.[16,19] Taken together, no unifying explanation for the TSK airspace phenotype that connects the matrix abnormalities with ongoing airspace enlargement has been offered.

We hypothesized that the genetically determined alteration in extracellular matrix composition in the TSK mouse might provide important data with regards to the mechanisms that link matrix abnormalities and destructive alveolar enlargement. We specifically explored the thesis that the TSK matrix abnormality does not require overt elastolysis, but rather oxidative stress and cell death to result in a hypoplastic lung. Here we show for the first time that the matrix alterations in the TSK lung promote susceptibility to postnatal oxidative stress and apoptosis which in combination support airspace simplification. Our data indicate that the TSK lung exemplifies a novel mechanism of genetic emphysema with oxidative stress and increased cell death resulting from matrix dysmorphogenesis.

Materials and Methods

Animal Studies

Tight-skin mice were obtained from Jackson Laboratory (Bar Harbor, ME) and subsequently backcrossed for >10 generations into a C57Bl/6 background to eliminate the *pallid* allele. Animals were allowed free access to food and water. The mice were housed in a facility accredited by the American Association of Laboratory Animal Care, and the animal studies were reviewed and approved by the institutional animal care and use committee of Johns Hopkins School of Medicine. Genotyping was performed as described.[20] For the *N*-acetylcysteine (NAC) administration studies, NAC (Sigma) was added to drinking water at doses equivalent to 2.5 g/kg/day for a 4-week long administration to adult mice (4 months of age). Drinking water was provided for control mice.

Morphology and Histology

Three to five mice of each genotype were studied at the noted ages. For histological and morphometric analyses, mouse lungs were inflated at a pressure of 25 cm H20 and fixed with 4% paraformaldehyde in low melt agarose. The lungs were equilibrated in cold 4% paraformaldehyde overnight, sectioned, and then embedded in paraffin wax. Sections were cut at 5 μm and either stained with H&E or processed for immunohistochemistry. Verhoeff-Van Gieson (VVG) staining was performed per standard protocol. Stained sections were assessed by light microscopy to elucidate pattern of staining reflective of elastin deposition.

Morphometry

Measurements were performed on H&E-stained sections taken at intervals throughout both lungs. Slides were coded, captured by an observer, and masked for identity. Ten to fifteen images per slide were acquired at $\times$10 magnification by an observer blinded to the experimental groups. Mean linear intercepts were assessed by digital morphometry with a macro operation using Metamorph Imaging Software (Universal Imaging, Molecular Devices, Downingtown, PA) and recorded as arbitrary units, as previously described.[21] The mean linear intercept (MLI) was determined using the average distance between intersects of approximately 40 lines interposed to the image.

Immunohistochemistry

Tissue sections were deparaffinized and rehydrated in an ethanol series. Sections were blocked for nonspecific

binding with 3% normal serum from chicken and incubated with the primary antibodies for 1 hour at room temperature. For immunofluorescence, sections were then incubated with secondary antibodies at 1:200 for 30 minutes at room temperature (Molecular Probes, Carlsbad, CA). Sections were counterstained with 4′,6′-diamidinio-2-phenylindole and mounted with Vectashield hard set mounting medium (Vector Labs). For immunohistochemistry, following incubation with the primary antibody overnight at 4°C, slides were washed with phosphate-buffered saline with Tween-20 (PBST), incubated with an appropriate biotinylated secondary antibody (Jackson ImmunoResearch) and developed by using avidin-biotinylated enzyme complex, 5-bromo-4-chloro-3-indolyl phosphate, and diaminobenzidine detection reagents (Vector Laboratories). Antibodies were used at the following concentrations: 8-hydroxyguanosine (mouse monoclonal, Santa Cruz, 1:100), Nitrotyrosine (mouse monoclonal, Abcam, 1:250), MAC-3 (rat monoclonal, BD Pharmingen, 1:100), Neutrophil (rat monoclonal, Serotec 1:50), proliferating cell nuclear antigen (rabbit polyclonal, Santa Cruz, 1:50), extracellular superoxide dismutase (EC-SOD, mouse monoclonal 4G11G6, generous gift from Tim Oury, and goat polyclonal, Santa Cruz, 1:50), and active caspase-3 (rabbit polyclonal, Abcam, 1:25). Quantitative immunohistochemistry was performed by normalizing staining to either total cell count or tissue area as indicated using Metamorph software. Since the TSK lungs are simplified and have less tissue per field, we normalized immunohistochemical staining for proteins that resided within a tissue structure to tissue area rather than cell count. By contrast, mitotic or apoptotic indices were normalized to nuclei as per convention. Images are captures using NIS Elements on the Nikon Upright Biological Microscope Model Eclipse 80i.

Western Blot Analysis

Whole lung lysates were extracted in M-Per buffer from Pierce. Protein concentrations were determined using the Biorad Protein Assay. Aliquots of 30 to 50 μg of protein were boiled and then loaded onto Tris-HCL gels and transferred electrophoretically to nitrocellulose membranes. Membranes were incubated with the primary antibody for 1 hour at room temperature. Detection was by the Pierce West Dura ECL detection system. Primary antibodies and dilutions were as follows: β-actin (rabbit polyclonal, Abcam, 1:1000), poly(ADP-ribose) polymerase (PARP)-1 (rabbit polyclonal, Abcam, 1:1000), EC-SOD (goat polyclonal, Santa Cruz, 1:200), active caspase 3 (rabbit polyclonal, Abcam 1:1000), total caspase 3 (rabbit monoclonal, Cell Signaling, 1:1000), active caspase 6 (rabbit monoclonal, Cell Signaling 1:1000), total caspase 6 (rabbit monoclonal, Cell Signaling 1:1000), active caspase 8 (mouse monoclonal, Cell Signaling, 1:1000), and total caspase 8 (rabbit polyclonal, Cell Signaling, 1:1000). Positive controls for caspases 3, 6, and 8 were from R&D.

Apoptosis Assays

Terminal deoxynucleotidyl transferase dUTP nick-end labeling (TUNEL) staining was performed using the Calbiochem TdT-FragEL DNA Fragmentation Detection Kit. Protocol supplied with kit was followed with minor modifications of incubation times. Antigen retrieval was performed for 10 minutes using Borg Decloaker RTU (Biocare Medical) followed by a standard avidin-biotinylated enzyme complex protocol. Detection of TUNEL-positive cells was evaluated using diaminobenzidine substrate (Dako Cytomation, Carpinteria, CA). Quantitation was performed as above. Caspase 3 activity was measured in whole lung lysates using the Promega Caspase Glo 3/7 Assay kit.

Zymography

Zymography was performed using Invitrogen Novex Mini Cell System. Samples were diluted in 2× zymogram sample buffer (Invitrogen, Carlsbad, CA). Fifty micrograms of lung lysates were loaded on 10% Gelatin zymogram gels (Invitrogen) and run at 125V. Ten nanograms of recombinant mouse MMP9 protein (R&D Systems, Minneapolis, MN) was loaded as positive control. Gels were washed in dH2O and incubated in 1× Novex Renaturing buffer (Invitrogen) for 30 minutes at room temperature. Gels were then washed in dH2O and equilibrated in 1× Novex Developing (Invitrogen) buffer for 30 minutes at room temperature. Gels were incubated overnight at 37°C in fresh 1× developing buffer followed by detection with SimplyBlue Safe Stain (Invitrogen).

Bromodeoxyuridine Labeling

Cell-specific proliferation was assessed after in adult TSK mice and age matched controls by determining the labeling index in the lung parenchyma using 5-bromo-2_-deoxyuridine (BrdU). Briefly, mice received two intraperitoneal injections of 1 ml/100g animal weight of BrdU labeling reagent (Zymed, San Francisco, CA) at a 2-hour interval. Lungs were harvested for immunohistochemistry 1 hour after the injection and subjected to immunostaining for BrdU. Cell specific staining was assessed by quantitative immunohistochemistry.

Oxidative Stress Assays

For the 2′,7′-dichlorofluorescein (DCF) analysis, lung tissue samples were quick frozen, weighed and stored at −80. Tissues were thawed on ice and homogenized in ice cold 40 mmol/L Tris-HCL and 0.1% Tween buffer (pH 7.4) using a handheld 1200 E polytron. An aliquot was reserved for protein analysis (BCA Protein Assay Kit, Pierce). The remaining was divided into two equal aliquots. One was loaded with a final concentration of 5 μmol/L 2′,7′-dichlorofluorescein diacetate (Molecular Probes). The other received equal volume of dimethyl sulfoxide to serve as a "blank" controlling for tissue autofluorescence. All samples were incubated for 15 minutes in a 37°C incubator. Fluorescence was determined at four time points post-incubation (0, 30, 60, and 90 minutes) using a Hitachi F2500 Fluorescence Spectrophotometer set at 504 nm excitation, and 529 nm emis-

sion (5 mm slits). Blank readings were subtracted from loaded sample readings, and values were presented as fluorescent units per milligram of protein or mg tissue. Unknown fluorescence values were standardized using known concentrations of DCF. Protocol modified from.[22]

To measure EC-SOD activity, lung lysates were prepared and analyzed with Superoxide Dismutase Assay Kit II (Calbiochem) according to instructions. Experiments were performed in triplicate.

Expression Profile Analysis

RNA isolation, microarray construction, and hybridization were previously described.[23] Briefly, NIA M17KA&B Arrays consisting of a set of 8448 spotted cDNAs, arrayed in duplicate, were printed on Nytran + Supercharge nylon membranes (Schleicher & Schuell, Keene, NH), and hybridized with [α-33P] dCTP-labeled cDNA probes overnight at 50°C as previously described.[24] Hybridized arrays were rinsed in 2× SSC and 0.1% SDS twice at 55°C followed by washes in 2× SSC and 0.1% SDS at 55°C. Microarrays were exposed for 1 to 3 days and scanned using a PhosphorImager (Molecular Dynamics, Sunnyvale, CA) at a 50-μm pixel resolution. ArrayPro software (MediaCybernetics, Silver Spring, MD) was used to convert the hybridization signals into raw intensity values; data generated were transferred into Microsoft Excel for further analysis.

Z-transformation for normalization was performed on each sample/array on a stand-alone basis, followed by the removal of non-named genes.[25] Significant changes in gene expression were calculated by Z test.[26] In addition, the mean difference of all calculated changes in gene expression was expressed in units of SD from the average change of all genes for that comparison and referred to as a Z ratio. Z ratios are a direct measure of the likelihood that an observed change is an outlier in an otherwise normal distribution and their use allows for the detection of large changes with high variance that might otherwise be missed by conventional significance testing. Significant gene lists were calculated by selecting genes that satisfied a significance threshold criteria of Z test P values less than or equal to 0.001 (10^{-3}), a false discovery rate less than or equal to 0.1, and either a fold change ±2.0 or greater, or a Z ratio values greater or less than ±2.0.

Statistical Analysis

Single factor analysis of variance and Student's t-tests were used to determine differences between groups. In the mor-

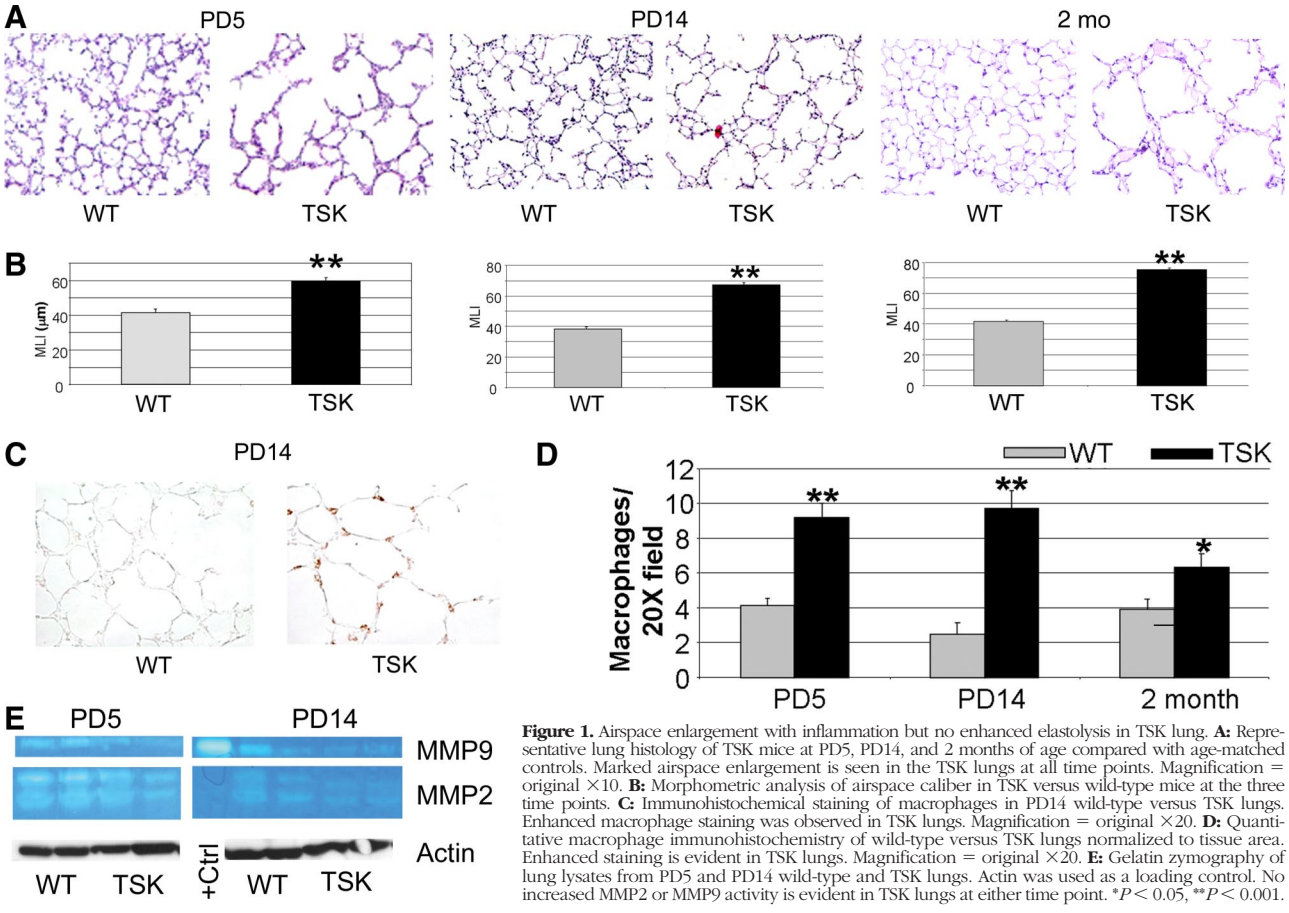

Figure 1. Airspace enlargement with inflammation but no enhanced elastolysis in TSK lung. **A:** Representative lung histology of TSK mice at PD5, PD14, and 2 months of age compared with age-matched controls. Marked airspace enlargement is seen in the TSK lungs at all time points. Magnification = original ×10. **B:** Morphometric analysis of airspace caliber in TSK versus wild-type mice at the three time points. **C:** Immunohistochemical staining of macrophages in PD14 wild-type versus TSK lungs. Enhanced macrophage staining was observed in TSK lungs. Magnification = original ×20. **D:** Quantitative macrophage immunohistochemistry of wild-type versus TSK lungs normalized to tissue area. Enhanced staining is evident in TSK lungs. Magnification = original ×20. **E:** Gelatin zymography of lung lysates from PD5 and PD14 wild-type and TSK lungs. Actin was used as a loading control. No increased MMP2 or MMP9 activity is evident in TSK lungs at either time point. $^{*}P < 0.05$, $^{**}P < 0.001$.

phometric study, statistical differences were determined by the unpaired student's *t*-test for comparison of septal measurements. A two-factor analysis of variance (genotype × time) was performed to assess for significant interaction with respect to the readouts of MLI, nitrotyrosine staining, and TUNEL staining using Sigmastat software (Systat). Values for all measurements were expressed as means ± SE, and *P* values for significance were designated at <0.05.

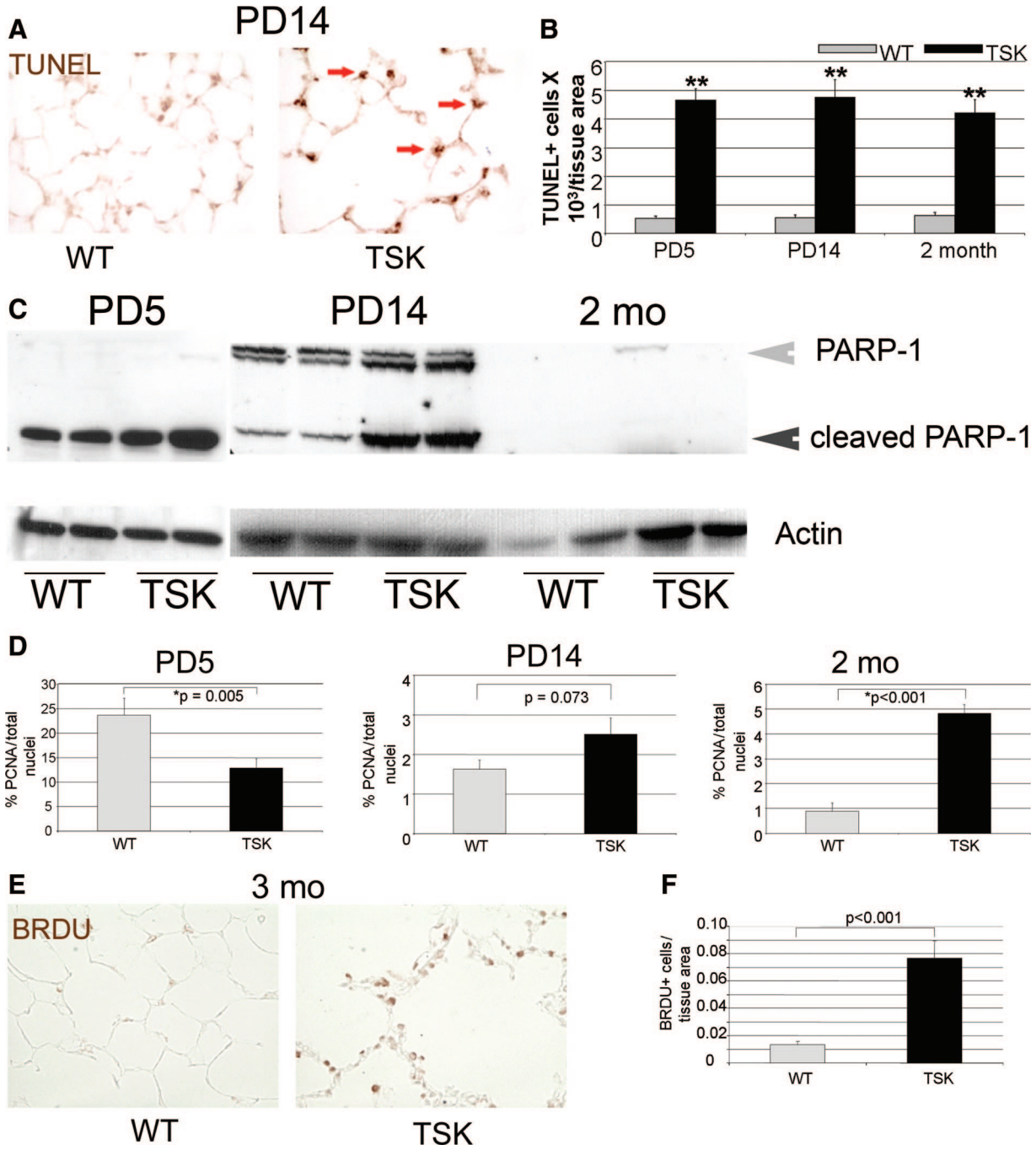

Figure 2. Prominent apoptosis with reduced proliferation in the neonatal TSK airspace. **A:** TUNEL staining of the PD14 wild-type and TSK lung shows enhanced epithelial cell death in the TSK airspace. **Arrows** denote sites of positive staining in the TSK lung. Magnification = original ×20. **B:** Quantitative immunohistochemistry shows maximal cell death in the PD5 TSK lung that decreases with time. **C:** Western blotting for PARP cleavage products in lysates from wild-type and TSK lungs at PD5, PD14, and 2 months of age. Increased PARP cleavage occurs during neonatal development in the TSK lung. Gray **arrowhead** indicates intact PARP-1 protein. Black **arrowhead** denotes PARP-1 cleavage product. Actin was used as a loading control. **D:** Quantitative immunohistochemistry of proliferating cell nuclear antigen staining normalized to total cell count in wild-type and TSK airspace at PD5, PD14, and 2 months of age. The mitotic index is reduced in the PD5 TSK airspace but increased by adulthood. **E:** Representative BRDu staining in adult wild-type versus TSK lungs. Increased BRDu labeling is observed in the TSK airspace. Magnification = original ×20. **F:** Quantitative immunohistochemistry of BRDu labeling confirms increased staining in the TSK lung. $^{*}P < 0.05$, $^{**}P < 0.001$.

Results

Airspace Morphology, Inflammation, and Metalloprotease Activation in Maturing TSK Mice

To establish the evolution of airspace abnormalities in TSK mice, we performed a temporal survey of the alveolar histology, morphometry, and macrophage abundance in these mice. Consistent with the findings of other groups, we detect early defects in septation that persist throughout adulthood (Figure 1, A and B). Specifically, the airspace caliber in TSK mice is 50%, 62%, and 78% greater than that of wild-type littermates at postnatal day 5 (PD5), PD14, and 2 months of age, respectively. Single factor analysis of variance demonstrated a significant contribution of genotype and time for MLI, $P < 0.001$ for each (see supplemental Table S1 at *http://ajp.amjpathol.org*). Furthermore, a two-factor analysis of variance showed a significant interaction between genotype and time ($P < 0.001$). We saw no difference in weight between the TSK mice and wild-type controls at any of the time points, suggesting equivalent nutritional status. Since inflammation can result in airspace destruction, we quantified macro-

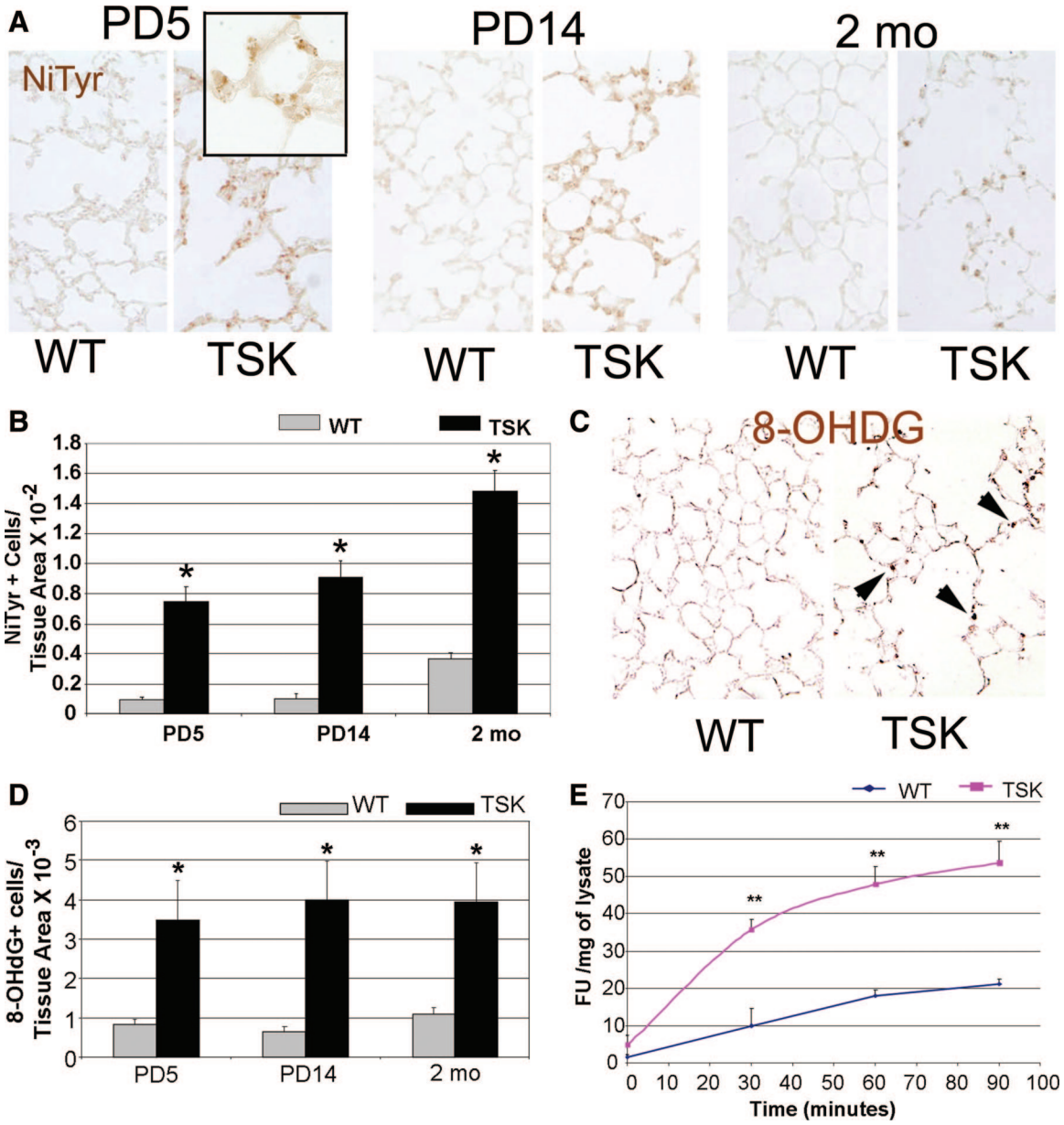

Figure 3. Increased oxidative and nitrosative stress in the TSK lung. **A:** Representative immunohistochemical staining for nitrotyrosine in wild-type and TSK lungs at PD5, PD14, and 2 months of age. Markedly enhanced staining is evident in the TSK lung at the three time points. **Inset** shows prominent airspace epithelial staining in the PD5 lung. Magnification = original ×20; ×60 (**inset**). **B:** Quantitative immunohistochemistry of nitrotyrosine shows enhanced staining in the TSK lung parenchyma. **C:** Representative 8-deoxyguanine immunohistochemistry in adult wild-type and TSK lungs showing increased staining in the TSK parenchyma. Magnification = original ×20. **Arrows** denote representative sites of staining in the airspace wall. **D:** Semiquantitative analysis of 8-hydroxyguanosine staining in adult wild-type and TSK lungs confirming increased staining in the TSK lungs. **E:** Time course of DCF liberation from lysates of PD5 wild-type and TSK mice. $^{*}P < 0.001$ and $^{**}P < 0.01$.

phages in the TSK lung by immunohistochemical staining and surveyed metalloprotease (MMP) activation by zymography and immunohistochemistry. Although we found increased macrophages in the TSK lung at PD5, PD14, and 2 months of age, zymographic analysis revealed no evidence of MMP 2 or MMP9 induction or activation at these same time points (Figure 1, C–E, data not shown). However, we did find increased MMP2 activation at PD5 in both wild-type and TSK mice compared with later time points, possibly reflecting temporally defined matrix remodeling. We similarly saw no significant induction of MMP12 by immunoblotting in the TSK lung (data not shown). Elastin deposition, as reflected by VVG staining, was preserved and of normal content in the TSK lung at all time points (see supplemental Figure S1 at *http://ajp.amjpathol.org*). Neutrophils, an alternative source of MMPs, were not increased in the TSK lung at PD5 or PD14 by immunohistochemical survey (data not shown). Taken together, our battery of studies did not demonstrate evidence of increased matrix turnover in the TSK lung.

Apoptosis and Proliferation in the TSK Lung

Since reduced septation can reflect enhanced apoptosis or reduced proliferation of cellular constituents of the airspace, we used *in situ* strategies to evaluate these processes in the TSK lung. We found increased TUNEL staining in the TSK airspace at all three time points, consistent with increased cell death (Figure 2, A and B). Single factor analysis of variance demonstrated a significant effect of either genotype or time on TUNEL staining. Of note, a two-factor analysis of variance analysis showed no significant interaction between genotype and time for this readout, distinct from the MLI result (see supplemental Table S1 at *http://ajp.amjpathol.org*). However, there was no increase in active caspase 3 by immunoblotting, immunohistochemical staining or luminescent activity assay (see supplemental Figure S2 at *http://ajp.amjpathol.org*). We also saw no enhanced caspase 6 or 8 activity by immunoblotting, other conventional markers of caspase-dependent apoptosis, in the developing and adult TSK lung (see supplemental Figure S2 at *http://ajp.amjpathol.org* and data not shown). PARP-1, is a nuclear enzyme activated by the DNA strand breaks that accompany certain forms of tissue injury.[27] We observed increased levels of cleaved PARP-1, a signature of apoptosis,[28] in the PD5 and 2-week TSK lung, implicating apoptotic signaling early in the evolution of the airspace lesion in the absence of overt destruction (Figure 2C). Adult TSK mice, by contrast, did not show evidence of PARP-1 cleavage despite evidence of ongoing cell death. Although our panel of studies did not demonstrate any evidence of caspase-dependent apoptosis, alternative caspase-dependent pathways may still be involved at any of the evaluated time points. Interestingly, even though enhanced cell death occurs in both developing and adult TSK lung, the mechanism of cell death, apoptosis in the developing and mixed apoptosis/necrosis in the adult, may be age-specific.

To establish whether reduced proliferation contributed to the airspace phenotype, we performed BrDU labeling in adult TSK mice and proliferating cell nuclear antigen immunostaining in developing and adult TSK mice. The proliferative profile of the TSK lung was highly reflective of developmental stage, with a reduced mitotic index present only in the PD5 lung (Figure 2E). By adulthood, increased proliferation was evident in the mutant lung, consistent with a compensatory response (Figure 2, D–F).

Oxidative Stress Injury in the TSK Lung

Observations from human and animal-based studies have shown that oxidative stress contributes to the airspace phenotype in acquired emphysema. Moreover, PARP-cleavage and apoptosis, two cell-death mechanisms detected in the TSK lung, can result from increased oxidative stress.[29,30] Whether oxidative stress is involved in airspace enlargement not associated with smoking or hyperoxic injury is unknown. Matrix components, in selective contexts, have also been shown to induce oxidative stress.[31] To establish whether the airspace lesion and apoptosis in the TSK lung reflected matrix-triggered oxidant injury, we examined both oxidative and nitrosative stress in the TSK lung at three different developmental time points. Histochemical staining for nitrotyrosine, a marker of nitrosative modification of cellular proteins, showed a significant and progressive enhancement in the TSK lung compared with wild-type controls (Figure 3, A and B). Single factor analysis of variance analysis showed a significant contribution of genotype to nitrotyrosine staining, but no significant contribution of time. Furthermore, two-way analysis of variance did not show any interaction between genotype and time for the measurement of oxidative stress (see supplemental Table S1 at *http://ajp.amjpathol.org*). The compound 8-hydroxyguanosine is a DNA base modified product that is generated by reactive oxygen species

Table 1. Antioxidant Expression Survey in PD14 Wild-Type vs TSK Lung

Class	Gene name	Fold change (TSK/WT)	*P* value
Glutathione synthesis	*GSS*	1.24	*NS
	GSR	1.09	NS
Glutathione conjugation	*GSTP2*	1.13	NS
	GSTM1	0.92	NS
	GSTM2	1.03	NS
	GSTM5	1.00	NS
Glutathione peroxidases	*GPX1*	1.06	NS
	GPX3	1.21	NS
	GPX4	1.10	NS
Peroxiredoxins	*PRDX1*	1.17	NS
	PRDX2	1.13	NS
	PRDX3	1.32	NS
	PRDX5	1.08	NS
	PRDX6	1.19	NS
Thioredoxins	*TXNRD1*	1.28	NS
	TXN1	0.93	NS
Superoxide dismutases	*SOD1*	1.13	NS
	SOD2	1.25	NS
Heme oxygenases	*HMOX1*	1.10	NS
	HMOX2	1.03	NS

*NS-Not significant.

and is another well accepted histological marker of oxidative stress.[32] *In situ* assessment of 8-hydroxyguanosine staining demonstrated a similar pattern of induction in the TSK lung (Figure 3, C and D). Dichlorofluorescin is a cell permeable fluorescein derivative that, on oxidation, forms DCF, a fluorescent compound that can be detected and quantified in whole cell systems.[33] Using the DCF assay as a biochemical measure of oxidative stress, we found increased DCF fluorescence in the mutant lung (Figure 3E). Assessment of the lung transcriptome of 2-week-old TSK mice did not implicate reduced local antioxidant expression as the primary cause of the enhanced oxidative stress (Table 1). In fact, this broad survey of antioxidant expression revealed no significant induction of any antioxidant in the TSK lung compared with wild-type controls. Thus, the airspace lesion is accompanied by the constellation of enhanced oxidative stress without a proportionate and responsive increase in antioxidant expression. These studies suggest that reactive oxidant species are generated early in the evolution of airspace simplification in the TSK lung.

To determine whether macrophages might be the source of the increased oxidative stress, we quantified markers of nitrosative stress in macrophages from PD5 and adult wild-type and TSK mice. We found a significant increase in the proportion of macrophages that expressed markers of oxidative stress in the TSK lung at both time points (Figure 4, A and B). However, when we looked at type II epithelial cells, we saw a greater proportion of cells with evidence of oxidative stress at PD5 and PD14 in the TSK lung compared with wild-type (360% and 50% increase, respectively, in the TSK relative to wild-type lung at the two time points) (Figure 4C). Given that macrophage number is markedly elevated in the TSK lung, the contribution of macrophages to the aggregate oxidative stress is likely of greater consequence in perpetuating rather than initiating the injury. Thus, the macrophages, while not liberating destructive proteases, are clearly contributing to the oxidative stress injury.

The early conflation of oxidative stress and apoptosis in the PD5 lung prompted the consideration that the transition to normoxia from the *in utero* hypoxic environment might represent a form of oxidant injury, recapitulating a mechanism of airspace simplification in lung disease of prematurity.[34] We examined markers of oxidative stress in the embryonic day 19 (ED19) and the PD1 lungs. We found no evidence of increased nitrotyrosine staining in the ED19 TSK lung (Figure 5, A and B). However, we did find increased oxidative stress in the PD1 TSK lung but no enhanced TUNEL staining (Figure 5, A–C). These data support postnatal ventilation in nor-

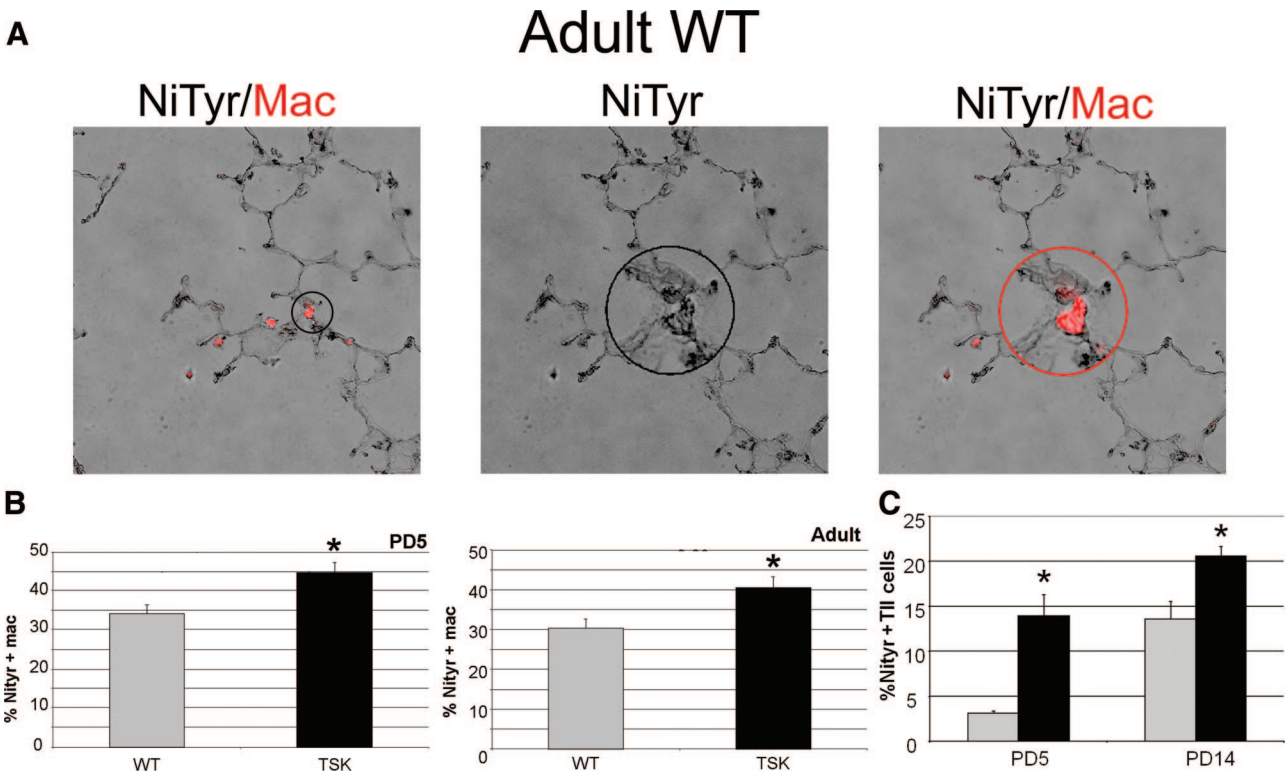

Figure 4. Macrophages and alveolar type II epithelial cells from TSK lung have increased oxidant stress. **A:** Representative immunofluorescent images demonstrating positive examples of nitrotyrosine (black) and macrophage (red) marker colocalization in an adult wild-type lung. The nitrotyrosine marker was detected using a diaminobenzidine substrate. The image was captured in color and converted to grayscale to enhance the contrast. The positive macrophage staining was detected using a fluorescent secondary and merged with the grayscale of nitrotyrosine to yield the final image showing the macrophage marker in red and the nitrotyrosine in black. **Left** image shows low power image of colocalized markers. Encircled insets in **middle** and **right** images show nitrotyrosine staining of a representative field (**middle**) and evidence of nitrotyroisine colocalization with macrophage marker (mac3, **right**) in the same field, respectively. Magnification = original ×20; ×60 (**inset**). **B:** Percentage of macrophages from wild-type and TSK lungs at PD5 (**left**) and 3 months of age (**right**) expressing the marker of nitrosative stress, nitrotyrosine. **C:** Percentage of type II epithelial cells from wild-type and TSK lungs at PD5 and PD14 expressing nitrotyrosine. NiTyr-nitrotyrosine immunostaining, Mac-mac3 immunostaining, $^{**}P < 0.001$, $^{*}P < 0.05$.

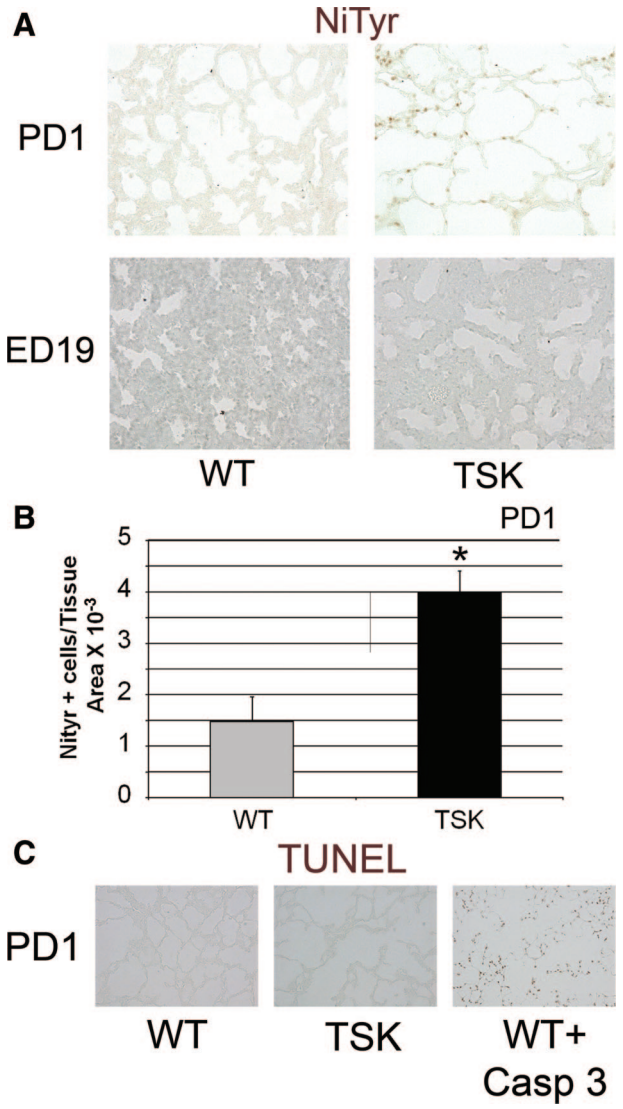

Figure 5. Early postnatal oxidant stress evident in TSK lung. **A:** Nitrotyrosine immunohistochemistry on ED19 and PD1 wild-type and TSK lungs. Increased staining is apparent in the PD1, but not ED19 TSK lung compared with age-matched controls. **B:** Quantitative analysis of staining shows a significant increase in nitrotyrosine staining in the lung parenchyma of ED19 TSK mice. **C:** TUNEL staining of PD1 wild-type and TSK lungs and age matched lungs treated with active caspase 3. No increased staining is apparent in PD1 TSK lungs compared with wild-type controls. $^{**}P < 0.001$, $^{*}P < 0.05$ Images all captured at ×20 magnification.

moxia as the probable oxidant trigger and the clear precedent to cell death in the neonatal lung.

Antioxidant Therapy Improves Oxidative Stress and Measures of Airspace Injury in TSK Mice

Oxidative stress induces apoptosis in ischemic brain injury and photoreceptor cell death models.[35,36] Our demonstration of increased oxidative stress in the TSK lung prompted us to investigate whether the airspace lesion is attributable to oxidant injury. To establish whether antioxidant therapy could improve morphometry in mice with established airspace enlargement, we used 3-week-old TSK mice with age-matched controls. TSK mice were treated with NAC, a thiol antioxidant with both glutathione-generating and oxidant-scavenging activities, for 4 weeks and then evaluated the lungs of these mice by morphometric analysis.[37] Doses that typically reverse oxidative stress in rodent models (~0.5 to 1 g/kg/d) were ineffective in the TSK mouse lung (data not shown). However, at very high doses, ~2.5 g/kg/d (>two-fold increase over the normal therapeutic dose), we found a significant reduction in oxidative stress in lungs of TSK mice, associated with a 12% improvement in airspace caliber and a 30% normalization of the airspace enlargement conferred by the TSK phenotype. Two-factor analysis of variance showed a significant interaction effect between genotype and NAC treatment ($P < 0.001$, $F = 31.562$), manifest in the improvement in airspace caliber in the adult TSK lung. These data implicate increased oxidant signaling as a critical upstream perturbation in the TSK lung (Figure 6, A–C). We also saw a trend toward improvement in apoptosis in the lungs of NAC-treated TSK mice, which was not statistically significant (Figure 6, D and E).

Since NAC treatment only partially attenuated the airspace enlargement in adult mice, we considered whether early perinatal treatment might result in a more significant rescue of airspace architecture. To optimize *in utero* and mammary delivery of NAC to the embryos and pups, respectively, we increased the concentration of NAC in the drinking water to 8.6 g/kg/day. When we administered NAC at this dose from time of conception, we were able to achieve a markedly greater improvement of airspace caliber at PD14, 26% absolute reduction and 67% normalization of airspace enlargement conferred by TSK phenotype (Figure 7, A and B). A two-way analysis of variance analysis did not show a significant interaction effect between genotype and perinatal NAC treatment. This result is consistent with the positive effects of NAC treatment on airspace caliber in both the developing wild-type and TSK lungs. Thus, the hyperoxic stress encountered during the prenatal to postnatal transition may have genotype-independent anti-alveolarization effects. These results suggest that early use of antioxidant interventions may have greater efficacy in disease phenotypes punctuated by developmental airspace enlargement.

Abnormal EC-SOD Deposition and Activity in the TSK Lung

Since we did not see any reduction in the expression of the major antioxidants in the lung by microarray analysis, we considered other possible explanation for the requirement of high doses of NAC to reverse oxidative stress. EC-SOD, an important superoxide anion scavenger in the extracellular matrix, is the most abundant superoxide dismutase in the lung.[38] EC-SOD binds to nonelastic elements of the extracellular matrix, namely collagen I and fibulin 5.[39,40] Given that both of these proteins show dysregulated deposition in the TSK lung, we considered whether the extracellular abundance of EC-SOD was similarly disturbed.[41] By immunoblotting, we found a no change in the abundance of EC-SOD in the murine lung at PD5 or 3 months of age (see supplemental Figure S3 at

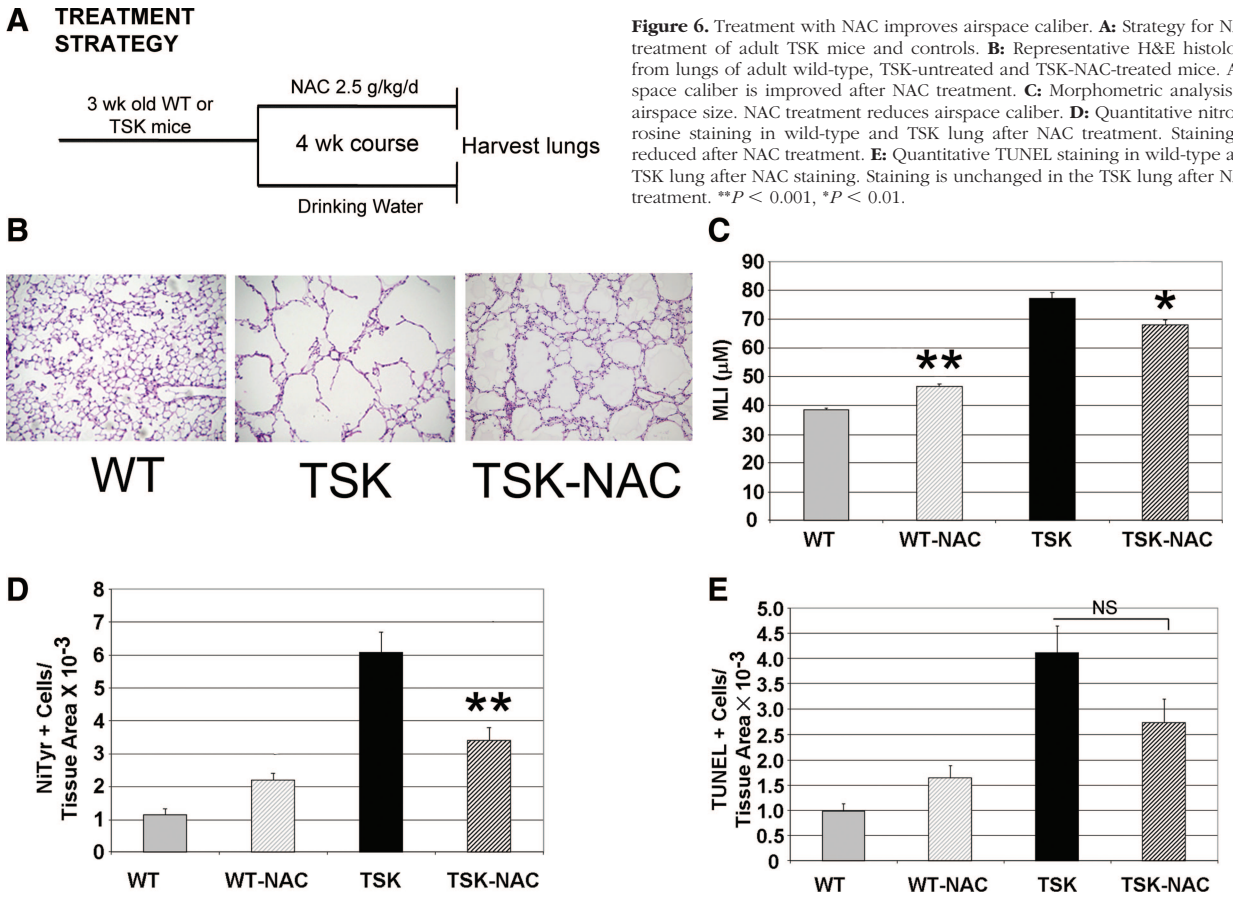

Figure 6. Treatment with NAC improves airspace caliber. **A:** Strategy for NAC treatment of adult TSK mice and controls. **B:** Representative H&E histology from lungs of adult wild-type, TSK-untreated and TSK-NAC-treated mice. Airspace caliber is improved after NAC treatment. **C:** Morphometric analysis of airspace size. NAC treatment reduces airspace caliber. **D:** Quantitative nitrotyrosine staining in wild-type and TSK lung after NAC treatment. Staining is reduced after NAC treatment. **E:** Quantitative TUNEL staining in wild-type and TSK lung after NAC staining. Staining is unchanged in the TSK lung after NAC treatment. $^{**}P < 0.001$, $^{*}P < 0.01$.

http://ajp.amjpathol.org). Immunohistochemical staining, however, showed fragmented and discontinuous deposition of ECSOD in the alveolar septae (Figure 8A). In addition, EC-SOD activity was reduced by 50% in TSK lung lysates (Figure 8B). Thus, altered EC-SOD deposition and activity in the TSK lung contributes to the exaggerated oxidative and nitrosative stress and, more importantly, is a direct consequence of the abnormal matrix associated with this phenotype. Furthermore, this reduced antioxidant availability plausibly contributes to the airspace enlargement observed in these mice without evidence of overt elastolysis.

Discussion

The central finding of the current study is that airspace enlargement in a murine model of genetic emphysema, TSK mouse, is partly attributable to postnatal oxidative stress injury and apoptosis, both triggered by matrix dysmorphogenesis in the absence of overt elastolysis. These data provide a novel insight into candidate mechanisms for alveolar simplification in disorders of the matrix, such as cutis laxa and Ehler-Danlos Syndrome. Additionally, this study establishes the proof of principle for the exploration of antioxidant modalities for the treatment of primary and acquired diseases of the matrix.

Because defects in either matrix deposition or homeostasis can result in airspace enlargement, an attractive hypothesis is that structural matrix abnormalities, with or without increased turnover, are sufficient to trigger increased airspace cellular turnover and oxidative stress. One mechanism for the airspace phenotype resulting from abnormal microfibrillar composition, as exemplified by fibrillin-1 deficient mice, implicates pro-apoptotic effects of excessive transforming growth factor (TGF)β signaling on resident alveolar cells but no primary abnormality in collagen or elastin deposition ([6] and unpublished observations). Even though enhanced TGFβ signaling plausibly accounts for the cutaneous phenotype of TSK mice, experimental support for TGFβ dysregulation as the predominant mechanism for the airspace enlargement has not been conclusive. Both haploinsufficiency for TGFβ1 and complete deletion of interleukin 4 (IL4), a potent local inducer of TGFβ1, significantly ameliorate the skin fibrosis, but have no effect on the airspace caliber.[42,43] Two alternative mechanisms, which are explored in this study, are that subtle matrix abnormalities 1) enhance oxidative stress with secondary cell death and 2) directly alter cellular attachments resulting in apoptosis.

Animal models of oxidative stress injury typically require a triggering exposure or insult such as hyperoxia, cigarette smoke, or infection. The exposure is frequently accompanied by compromised antioxidant protection, which culminates in organismal or tissue-specific injury. In the TSK lung, the apparent triggering insult is postnatal ventilation. Since the *in utero* environment is relatively

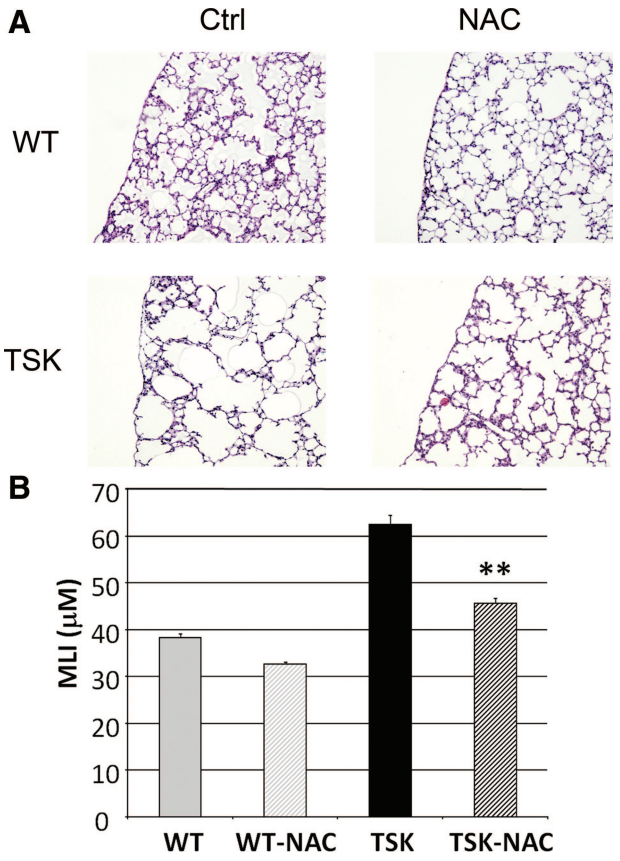

Figure 7. Prenatal treatment with NAC protects against airspace enlargement. **A:** Representative H&E images of PD14 TSK and control mice treated with high dose NAC or water from time of conception. Preservation of airspace architecture is evident in the TSK lung. **B:** Morphometric analysis of airspace size in TSK and control mice treated with NAC or water. Ctrl-oral water treatment, NAC-NAC treatment, $^{**}P < 0.001$. Images all captured at ×20 magnification.

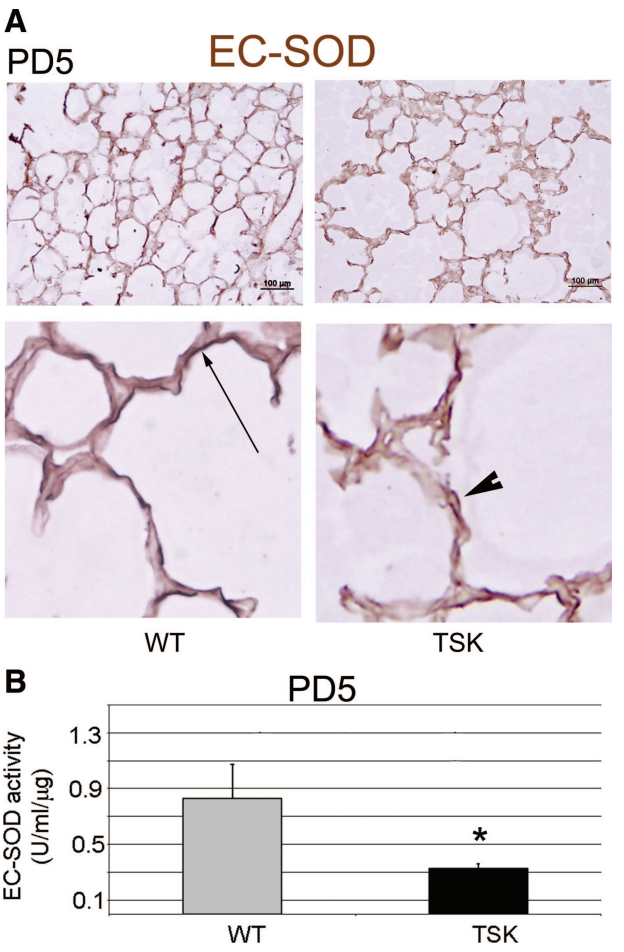

Figure 8. Abnormal EC-SOD deposition and activity in the TSK lung. **A:** Representative immunohistochemical staining of EC-SOD in the PD5 wild-type versus TSK lung. **Top** panel: Low power image demonstrating intact linear staining along alveolar walls in wild-type lungs but marked discontinuity and fragmentation in the TSK lung. Scale bar = 100 μm. **Bottom** panel: High power view emphasizes fragmentation of EC-SOD in the TSK lung. **Arrow** depicts continuous EC-SOD staining in the wild-type lung. **Arrowhead** shows fragmented staining pattern in TSK lung. Magnification = original ×100. **B:** EC-SOD activity in PD5 lung lysates. Reduced EC-SOD activity is detected in PD5 TSK lung compared with age-matched wild-type lungs. $^{*}P < 0.05$.

hypoxic, the transition to normoxia may be sensed as a hyperoxic insult in the TSK milieu. We invoke two novel mechanisms that follow from the primary matrix alteration, which can serve to escalate oxidant injury. First, since EC-SOD activity is reduced in the TSK lung, the local antioxidant quotient might not sufficiently titrate physiological superoxide production. Second, alveolar cell death secondary to oxidative stress can overload airspace clearance mechanisms and lead to increased oxidant production by resident phagocytes. Since appropriate apoptotic cell removal is critical to airspace homeostasis, deficient phagocyte function or capacity can result in defective lung repair.[44,45] Both mechanisms are probably operative in the TSK mouse since mice deficient in EC-SOD do not display basal oxidative stress (ie, loss of EC-SOD is not sufficient for oxidant injury under normal conditions) and NAC therapy only partially restores alveolar architecture in our studies (perhaps reflecting persistence of priming apoptotic insult).[46] Whether oxidative stress is a typical component of apoptosis has not been previously explored, but is a tempting unifying concept for the TSK lung phenotype. Recently, Tuder found that oxidative stress was a critical mediator in a murine model of emphysema produced by vascular endothelial growth factor blockade.[45] Similarly, we also detected enhanced PARP cleavage in the PD5 and the PD14 TSK lung, time points marked by appreciable oxidative stress injury in the lung. A model conflating matrix-triggered oxidative stress and cell death may also explain the airspace simplification reported in elastin-deficient, fibulin 5-deficient, and lysyl oxidase like 1-deficient mice, which all have profound airspace enlargement without inflammation or evidence of local proteolysis.[4,5,7,8] Findings by others of 1) elevated elastase expression in the adult TSK lung[12] and 2) increased airspace size in neonatal TSK mice without accompanying destructive stigmata,[11] also support an elegant model of abnormal matrix-triggered oxidative stress and apoptosis as the initial lesions that can predispose to subsequent proteolytic injury. This model was recently proposed by Shapiro as reconciling the dual observations of apoptosis and matrix turnover in human and murine emphysema.[47] Although our data suggests that there is no increased activation of the potent elastases

MMP2 and MMP9 in the TSK lung, we have not formally ruled out the activation of other non- or weakly gelatinolytic enzymes such as MMP12 as contributing to the evolution of airspace enlargement in the TSK lung. Furthermore, our statistical analysis implicating a genotype by age interaction for airspace caliber, but not for either oxidative stress or apoptosis, underscores mechanistic complexity in the relationship between the two measures of injury and the architectural phenotype.

Apoptotic cell loss in the airspace occurs during postnatal lung development and participates in the creation of the thin alveolar walls required for efficient gas exchange. The triggers for these physiological events in the airspace are unknown. Our linkage of matrix dysmorphology and abnormalities in microfibrillar structure to oxidative stress and apoptosis suggests that developmental matrix remodeling may represent a critical trigger for physiological septal thinning. Accordingly, primary or acquired abnormalities in matrix composition during the neonatal period can result in an exaggeration of this process with consequential pathological airspace enlargement. In fibrillin-1 deficient mice, we reported increased TGFβ-mediated postnatal apoptosis that resulted in airspace enlargement.[6] Our current findings in the TSK lung suggest that the initiator of apoptosis is not as important as the neonatal timing of the insult. Taken together, these genetic emphysema models support the "critical interval" hypothesis advanced by Massaro et al.[1]

We show two temporally defined mechanisms of cell death in the TSK lung: apoptosis and necrosis. Necrotic and apoptotic cell death frequently coexist in the simplified lung (best described in whole cell studies and acquired emphysema models).[48–51] Our PARP cleavage data only shows that the apoptotic component is more prominent in the developing and maturing airspace, when compared with the adult airspace. We postulate that since apoptosis is a known physiological process in the maturing lung and supports the septal thinning required for efficient gas exchange, an exaggeration of this process (here in the TSK lung) is more likely to be manifest in the developing context.[52] Our lab is currently dissecting the various cell death mechanisms that promote this exaggeration as well as the nonapoptotic mechanisms that may contribute to cell death in the adult TSK lung.

Susceptibility to the transition from an *in utero* to a postnatal environment is a feature of lung disease of prematurity, also termed bronchopulmonary dysplasia.[34] The vulnerable substrate is postulated to be the premature state of the lung and the inadequate expression of antioxidants. Our ability to mimic this triggering injury by expressing an abnormal matrix protein elevates the role of matrix dysmorphology, an underexplored compartment, in this disorder. Studies focusing on the matrix composition of the premature lung and models of bronchopulmonary dysplasia should be pursued and may possibly identify targets for intervention.

In conclusion, we show that the deposition of an abnormal matrix component, TSK fibrillin-1, is sufficient to confer susceptibility to postnatal oxidative stress and trigger excess cell death, culminating in airspace enlargement. We also demonstrate a blunted antioxidant response and impaired EC-SOD deposition in the TSK lung, which likely contributes to the oxidant injury. The induction of these canonical lung injury cascades in the absence of significant protease activation supports an intimate interaction between the matrix and lung homeostatic mechanisms. Our finding that NAC partially reverses the airspace enlargement of the TSK lung in an age-dependent matter further implicates the critical contribution of oxidative stress to the distal lung phenotype observed in primary matrix disorders. These results may reconcile the triangular pathogenetic paradigm of human emphysema involving matrix dysmorphology, oxidative stress, and apoptosis. Our findings also suggest that strategies to antagonize oxidant stress may avert or ameliorate the complex and robust destructive cascades that contribute to human emphysema. Future exploration of antioxidant therapies in other models of disturbed matrix deposition should also be pursued.

Acknowledgments

We thank Peter Henson, Dean Sheppard, Robert Senior, Landon King, Ari Zaiman, and Sharon McGrath-Morrow for careful reading of the manuscript; Hal Dietz and Steve Shapiro for helpful advice; Elizabeth Wagner and Julie Nijmeh for technical assistance with the DCF Assay; Roger Johns and Qingning Su for their assistance with the mouse embryo harvests; and Tim Oury for providing the ECSOD antibody.

References

1. Massaro D, Teich N, Maxwell S, Massaro GD, Whitney P: Postnatal development of alveoli. Regulation and evidence for a critical period in rats, J Clin Invest 1985, 76:1297–1305
2. Warburton D, Gauldie J, Bellusci S, Shi W: Lung development and susceptibility to chronic obstructive pulmonary disease. Proc Am Thorac Soc 2006, 3:668–672
3. Foronjy RF, Okada Y, Cole R, D'Armiento J: Progressive adult-onset emphysema in transgenic mice expressing human MMP-1 in the lung. Am J Physiol Lung Cell Mol Physiol 2003, 284:L727–L737
4. Liu X, Zhao Y, Gao J, Pawlyk B, Starcher B, Spencer JA, Yanagisawa H, Zuo J, Li T: Elastic fiber homeostasis requires lysyl oxidase-like 1 protein. Nat Genet 2004, 36:178–182
5. Nakamura T, Lozano PR, Ikeda Y, Iwanaga Y, Hinek A, Minamisawa S, Cheng CF, Kobuke K, Dalton N, Takada Y, Tashiro K, Ross Jr J, Honjo T, Chien KR: Fibulin-5/DANCE is essential for elastogenesis in vivo. Nature 2002, 415:171–175
6. Neptune ER, Frischmeyer PA, Arking DE, Myers L, Bunton TE, Gayraud B, Ramirez F, Sakai LY, Dietz HC: Dysregulation of TGF-beta activation contributes to pathogenesis in Marfan syndrome. Nat Genet 2003, 33:407–411
7. Wendel DP, Taylor DG, Albertine KH, Keating MT, Li DY: Impaired distal airway development in mice lacking elastin. Am J Respir Cell Mol Biol 2000, 23:320–326
8. Yanagisawa H, Davis EC, Starcher BC, Ouchi T, Yanagisawa M, Richardson JA, Olson EN: Fibulin-5 is an elastin-binding protein essential for elastic fibre development in vivo. Nature 2002, 415: 168–171
9. Green MC, Sweet HO, Bunker LE: Tight-skin, a new mutation of the mouse causing excessive growth of connective tissue and skeleton. Am J Pathol 1976, 82:493–512
10. Sakai LY, Keene DR, Engvall E: Fibrillin, a new 350-kD glycoprotein, is a component of extracellular microfibrils. J Cell Biol 1986, 103: 2499–2509

11. Martorana PA, van Even P, Gardi C, Lungarella G: A 16-month study of the development of genetic emphysema in tight-skin mice. Am Rev Respir Dis 1989, 139:226–232
12. de Santi MM, Gardi C, Martorana PA, van Even P, Lungarella G: Immunoelectron-microscopic demonstration of elastase in emphysematous lungs of tight-skin mice. Exp Mol Pathol 1989, 51:18–30
13. Gardi C, Cavarra E, Calzoni P, Marcolongo P, de Santi M, Martorana PA, Lungarella G: Neutrophil lysosomal dysfunctions in mutant C57 Bl/6J mice: interstrain variations in content of lysosomal elastase, cathepsin G and their inhibitors. Biochem J 1994, 299 (Pt 1):237–245
14. Rossi GA, Hunninghake GW, Gadek JE, Szapiel SV, Kawanami O, Ferrans VJ, Crystal RG: Hereditary emphysema in the tight-skin mouse. Evaluation of pathogenesis. Am Rev Respir Dis 1984, 129:850–855
15. Gardi C, Martorana PA, de Santi MM, van Even P, Lungarella G: A biochemical and morphological investigation of the early development of genetic emphysema in tight-skin mice. Exp Mol Pathol 1989, 50:398–410
16. Ito S, Bartolak-Suki E, Shipley JM, Parameswaran H, Majumdar A, Suki B: Early emphysema in the tight skin and pallid mice: roles of microfibril-associated glycoproteins, collagen, and mechanical forces. Am J Respir Cell Mol Biol 2006, 34:688–694
17. Szapiel SV, Fulmer JD, Hunninghake GW, Elson NA, Kawanami O, Ferrans VJ, Crystal RG: Hereditary emphysema in the tight-skin (Tsk/+) mouse. Am Rev Respir Dis 1981, 123:680–685
18. Starcher B, James H: Evidence that genetic emphysema in tight-skin mice is not caused by neutrophil elastase. Am Rev Respir Dis 1991, 143:1365–1368
19. Wallace VA, Kondo S, Kono T, Xing Z, Timms E, Furlonger C, Keystone E, Gauldie J, Sauder DN, Mak TW, Paige CJ: A role for CD4+ T cells in the pathogenesis of skin fibrosis in tight skin mice. Eur J Immunol 1994, 24:1463–1466
20. Denton CP, Zheng B, Shiwen X, Zhang Z, Bou-Gharios G, Eberspaecher H, Black CM, de Crombrugghe B: Activation of a fibroblast-specific enhancer of the proalpha2(I) collagen gene in tight-skin mice. Arthritis Rheum 2001, 44:712–722
21. McGrath-Morrow S, Rangasamy T, Cho C, Sussan T, Neptune E, Wise R, Tuder RM, Biswal S: Impaired lung homeostasis in neonatal mice exposed to cigarette smoke. Am J Respir Cell Mol Biol 2008, 38:393–400
22. Fontella FU, Siqueira IR, Vasconcellos AP, Tabajara AS, Netto CA, Dalmaz C: Repeated restraint stress induces oxidative damage in rat hippocampus. Neurochem Res 2005, 30:105–111
23. Barrett T, Cheadle C, Wood WB, Teichberg D, Donovan DM, Freed WJ, Becker KG, Vawter MP: Assembly and use of a broadly applicable neural cDNA microarray. Restor Neurol Neurosci 2001, 18:127–135
24. Cheadle C, Vawter MP, Freed WJ, Becker KG: Analysis of microarray data using Z score transformation. J Mol Diagn 2003, 5:73–81
25. Cheadle C, Cho-Chung YS, Becker KG, Vawter MP: Application of z-score transformation to Affymetrix data. Appl Bioinformatics 2003, 2:209–217
26. Nadon R, Shoemaker J: Statistical issues with microarrays: processing and analysis. Trends Genet 2002, 18:265–271
27. Chiarugi A: Poly(ADP-ribose) polymerase: killer or conspirator? The 'suicide hypothesis' revisited, Trends Pharmacol Sci 2002, 23: 122–129
28. Yu SW, Wang H, Poitras MF, Coombs C, Bowers WJ, Federoff HJ, Poirier GG, Dawson TM, Dawson VL: Mediation of poly(ADP-ribose) polymerase-1-dependent cell death by apoptosis-inducing factor. Science 2002, 297:259–263
29. Pagano A, Pitteloud C, Reverdin C, Metrailler-Ruchonnet I, Donati Y, Barazzone Argiroffo C: Poly(ADP-ribose)polymerase activation mediates lung epithelial cell death in vitro but is not essential in hyperoxia-induced lung injury. Am J Respir Cell Mol Biol 2005, 33:555–564
30. Liu PL, Chen YL, Chen YH, Lin SJ, Kou YR: Wood smoke extract induces oxidative stress-mediated caspase-independent apoptosis in human lung endothelial cells: role of AIF and EndoG. Am J Physiol Lung Cell Mol Physiol 2005, 289:L739–L749
31. Edderkaoui M, Hong P, Vaquero EC, Lee JK, Fischer L, Friess H, Buchler MW, Lerch MM, Pandol SJ, Gukovskaya AS: Extracellular matrix stimulates reactive oxygen species production and increases pancreatic cancer cell survival through 5-lipoxygenase and NADPH oxidase. Am J Physiol Gastrointest Liver Physiol 2005, 289: G1137–G1147
32. Ames BN, Shigenaga MK, Hagen TM: Oxidants, antioxidants, and the degenerative diseases of aging. Proc Natl Acad Sci USA 1993, 90:7915–7922
33. Wang H, Joseph JA: Quantifying cellular oxidative stress by dichlorofluorescein assay using microplate reader. Free Radic Biol Med 1999, 27:612–616
34. Asikainen TM, White CW: Pulmonary antioxidant defenses in the preterm newborn with respiratory distress and bronchopulmonary dysplasia in evolution: implications for antioxidant therapy. Antioxid Redox Signal 2004, 6:155–167
35. Lohr HR, Kuntchithapautham K, Sharma AK, Rohrer B: Multiple, parallel cellular suicide mechanisms participate in photoreceptor cell death. Exp Eye Res 2006, 83:380–389
36. Stefanis L: Caspase-dependent and -independent neuronal death: two distinct pathways to neuronal injury. Neuroscientist 2005, 11:50–62
37. Cotgreave IA: N-acetylcysteine: pharmacological considerations and experimental and clinical applications. Adv Pharmacol 1997, 38:205–227
38. Fattman CL, Schaefer LM, Oury TD: Extracellular superoxide dismutase in biology and medicine. Free Radic Biol Med 2003, 35:236–256
39. Nguyen AD, Itoh S, Jeney V, Yanagisawa H, Fujimoto M, Ushio-Fukai M, Fukai T: Fibulin-5 is a novel binding protein for extracellular superoxide dismutase. Circ Res 2004, 95:1067–1074
40. Petersen SV, Oury TD, Ostergaard L, Valnickova Z, Wegrzyn J, Thogersen IB, Jacobsen C, Bowler RP, Fattman CL, Crapo JD, Enghild JJ: Extracellular superoxide dismutase (EC-SOD) binds to type i collagen and protects against oxidative fragmentation. J Biol Chem 2004, 279:13705–13710
41. Gardi C, Martorana PA, Calzoni P, van Even P, de Santi MM, Cavarra E, Lungarella G: Lung collagen synthesis and deposition in tight-skin mice with genetic emphysema. Exp Mol Pathol 1992, 56:163–172
42. Kodera T, McGaha TL, Phelps R, Paul WE, Bona CA: Disrupting the IL-4 gene rescues mice homozygous for the tight-skin mutation from embryonic death and diminishes TGF-beta production by fibroblasts, Proc Natl Acad Sci USA 2002, 99:3800–3805
43. McGaha T, Saito S, Phelps RG, Gordon R, Noben-Trauth N, Paul WE, Bona C: Lack of skin fibrosis in tight skin (TSK) mice with targeted mutation in the interleukin-4R alpha and transforming growth factor-beta genes, J Invest Dermatol 2001, 116:136–143
44. Henson PM, Vandivier RW, Douglas IS: Cell death, remodeling, and repair in chronic obstructive pulmonary disease? Proc Am Thorac Soc 2006, 3:713–717
45. Kirkham P: Oxidative stress and macrophage function: a failure to resolve the inflammatory response. Biochem Soc Trans 2007, 35:284–287
46. Carlsson LM, Jonsson J, Edlund T, Marklund SL: Mice lacking extracellular superoxide dismutase are more sensitive to hyperoxia. Proc Natl Acad Sci USA 1995, 92:6264–6268
47. Tuder RM, Zhen L, Cho CY, Taraseviciene-Stewart L, Kasahara Y, Salvemini D, Voelkel NF, Flores SC: Oxidative stress and apoptosis interact and cause emphysema due to vascular endothelial growth factor receptor blockade. Am J Respir Cell Mol Biol 2003, 29:88–97
48. Shapiro SD, Ingenito EP: The pathogenesis of chronic obstructive pulmonary disease: advances in the past 100 years. Am J Respir Cell Mol Biol 2005, 32:367–372
49. Slebos DJ, Ryter SW, van der Toorn M, Liu F, Guo F, Baty CJ, Karlsson JM, Watkins SC, Kim HP, Wang X, Lee JS, Postma DS, Kauffman HF, Choi AM: Mitochondrial localization and function of heme oxygenase-1 in cigarette smoke-induced cell death. Am J Respir Cell Mol Biol 2007, 36:409–417
50. van der Toorn M, Slebos DJ, de Bruin HG, Leuvenink HG, Bakker SJ, Gans RO, Koeter GH, van Oosterhout AJ, Kauffman HF: Cigarette smoke-induced blockade of the mitochondrial respiratory chain switches lung epithelial cell apoptosis into necrosis. Am J Physiol Lung Cell Mol Physiol 2007, 292:L1211–L1218
51. Wickenden JA, Clarke MC, Rossi AG, Rahman I, Faux SP, Donaldson K, MacNee W: Cigarette smoke prevents apoptosis through inhibition of caspase activation and induces necrosis. Am J Respir Cell Mol Biol 2003, 29:562–570
52. Schittny JC, Djonov V, Fine A, Burri PH: Programmed cell death contributes to postnatal lung development. Am J Respir Cell Mol Biol 1998, 18:786–793